Series of Hydrated Lanthanide (La, Ce, Pr, Dy, Yb) Pyromellitate 3D Coordination Polymer with Tunnels Encapsulating Dimethylammonium Species and Its Crystal-to-Crystal Transformation upon Dehydration

Amandine Flament, Sylvain Duval, Natacha Henry, Christophe Volkringer, Fabrice Salles, Christelle Tamain, Thierry Loiseau

Series of hydrated lanthanide (La, Ce, Pr, Dy, Yb) pyromellitate 3D coordination polymer with tunnels encapsulating dimethylammonium species and its crystal-to-crystal transformation upon dehydration

Amandine Flament,[a,b] Sylvain Duval,[*,a] Natacha Henry,[a] Christophe Volkringer,[a] Fabrice Salles,[c] Christelle Tamain,[b] Thierry Loiseau[a]

[a] Univ. Lille, CNRS, Centrale Lille, Univ. Artois, UMR 8181 - UCCS - Unité de Catalyse et Chimie du Solide, F-59000 Lille, France.
[b] CEA, DES, ISEC, DMRC, Univ Montpellier, Marcoule, France.
[c] ICGM, CNRS, Univ. Montpellier, ENSCM, Montpellier, France.

Corresponding author: sylvain.duval@univ-lille.fr

Abstract

Synthesis and characterization of two distinct structural types of coordination polymers are reported with 1,2,4,5-benzenetetracarboxylate (btec) ligands associated to lanthanides (Ln) Ce(III), La(III) and Pr(III) for compounds **1-3**, and Dy(III) and Yb(III) for compounds **4-5**. The two structures are built from the connection of lanthanide centers with the linkers to construct 3D framework composed of 1D tunnels encapsulating dimethylammonium and water in $(CH_3)_2NH_2[Ln(btec)]\cdot 2H_2O$ (**1-3**) or dimethylammonium only in $(CH_3)_2NH_2[Ln(btec)(H_2O)]$ (**4-5**). These two atomic arrangements differ by the occurrence of infinite chains of edge-sharing $\{LnO_9\}$ units and, presence of trapped water species in **1-3**, instead of dinuclear carboxylate bridged $\{2 \times LnO_8\}$ units and, bonded aquo species to Ln centers in **4-5**. The dehydration process was investigated for compound **1**. Removal of water induces a crystalline phase transition related to the shrinkage of the 3D network to form $([Ln(btec)]\cdot(CH_3)_2NH_2$, noted **1'**). Elucidation of the mechanism is provided by combining water adsorption measurements with GCMC calculations. This transformation shows a relative flexibility of the network (cell volume variation of -6%) reminiscent of the breathing effect reported in MOF such as the MIL-53 series. The anhydrous phase **1'** is able to adsorb reversibly water as experienced with the measurement of water vapor isotherms.

Keywords : lanthanide(III) ; La, Ce, Pr, Dy, Yb, pyromellitic acid, coordination polymer, XRD structure,

Introduction

The research of crystalline coordination polymers (CP) and Metal-Organic Frameworks (MOF) has been intensively investigated for the last two decades. Indeed, this class of multifunctional materials has emerged due to their high surface areas porosity properties, resulting in a broad variety of applications such as gas storage and separation, catalysis, sensors, environmental remediation and drug delivery.[1–4] These solid compounds are constructed from the linkage of metallic centers, which can be isolated as polynuclear oxo clusters, with O- and/or N-donor organic ligands, through carboxylate- or N-bondings in order to build well-ordered structural topologies with different dimensionalities that can lead to tunable pores/channels and surface functionalities. Among the choice of potential metal elements from periodic table, the incorporation of lanthanide ions within the coordination polymers or MOFs structures imparts attracting properties. This particular series characterized by their unique electronic configurations and 4*f*-electron richness, introduces desirable features such as luminescence, [5–8] magnetic behavior [9] or catalytic activity [10,11] into the hybrid organic-inorganic network. Next to the choice of metal, the diversity offered by the richness of the organic molecule's library is at the origin of a very large number of works.

In this work, we focused our attention on the use of the polydentate linkers such as the pyromellitate ligand (benzene -1,2,4,5-tetracarboxylate, also named btec), which serves as an excellent bridging moiety due to its ability to coordinate metal ions in an expected robust manner, with multiple connection configurations.[12] Its association with lanthanides represents a sub-class of lanthanide-based MOF-like structures, and has been intensively studied since literature reported the formation of large number of coordination polymers exhibiting a wide variety of combination of lanthanides with different protonation states of the btec molecule.

It includes the Ln/btec ratio of 1/1, with the series [Ln(Hbtec)] (Ln = Ce-Nd, Sm-Dy, Er),[13–18] built up from the connection of infinite chains of edge-sharing {LnO_9} units with monoprotonated btec linkers in a 3D framework. A second structural type with the same Ln/btec ratio of 1/1 is encountered in the series [Ln_2(btec)(H_2btec)] corresponding to two distinct protonation states for the btec linkers. It was reported with the lanthanides La,[19,20] Ce, [21–24] Nd [17,25,26] and Sm, [27] and its crystal structure corresponds to a 3D network involving dimers of edge-sharing {LnO_9} units with either fully connected btec species or H_2btec species with two remaining no-bonded C-OH groups. A third similar Ln/btec ratio of 1/1 is found in a tetrahydrate form with the chemical formula [Ln_2(btec)(H_2btec)]·4H_2O, from Ln = Sm up to Er (except Ho). [28–34] It constructs a 3D structure with infinite chains of edge-sharing {$LnO_8(H_2O)$} units associated with two distinct types of pyromellitate ligands, in a non-protonated state (btec), which is fully linked to Ln centers through carboxylate arms, and a second one in a diprotonated state (H_2btec) with only two carboxylate arms (over 4) linking the lanthanide centers. Free water species are found trapped within narrow channels of the framework. With the same [Ln_2(btec)(H_2btec)] chemical formula, a second phase has been isolated with a different hydration state i.e 2.5H_2O (instead of 4) in the [Sm_2(btec)(H_2btec)]·4H_2O compound.[35] For this unique case, the crystal structure exhibits a layered net intercalated by free water molecules, with the connection of infinite chains of edge-sharing {LnO_9} units with btec linkers, one of them (in H_2btec form) linking samarium centers through carboxylate groups in 1,5 position (the other btec adopts a full connection through its all four carboxylate arms with Sm). For all these compounds, the pyromellitate ligand is observed in poly-protonated states,

with the combination of non-protonated together with protonated forms in most cases. Due to the number of four potential anionic charges (fully deprotonated state) expected for the tetratopic organic moiety, the Ln/btec stoichiometry converges to $[Ln_4(btec)_3]$ for a neutral network when combined with trivalent lanthanides. Indeed, various 4Ln/3btec structures topologies have been identified depending on the hydration states, which induces different crystalline arrangements. The lowest water content was reported in $[Eu_4(btec)_3(H_2O)_2]$, consisting of inorganic sheets of corner-sharing $[EuO_8(H_2O)$ or $Eu_9(H_2O)]$ units linked through the btec species.[36] A second series with hydration rate in the range 4-8 H_2O occurs with lanthanides corresponding to La, Ce,[37,38] mixed Nd/Yb [25] and Er [31,33] and is related to the $[Ln_4(btec)_3(H_2O)_8]\cdot nH_2O$. Their structures are built up from the connection of $\{LnO_9 / LnO_{10}\}$ tetrameric bricks forming a 3D framework with trapped water molecules. A third series with higher water content of $[Ln_4(btec)_3(H_2O)_{16}]\cdot 12H_2O$ (Ln = Sm,[39] Eu, [40] and Gd [30]) exhibits 3D arrangements of isolated monomeric $\{LnO_9\}$ or dimeric edge-sharing $\{Ln_2O_{16}\}$ units. With heavier lanthanides, such as erbium or thulium, only isolated $\{LnO_8\}$ units are found in 3D networks, as observed in the $[Er_4(btec)_3(H_2O)_{12}]\cdot 11\text{-}12H_2O$ [41,42] or $[Tm_4(btec)_3(H_2O)_{10}]\cdot 16H_2O$ compounds.[42] An alternative layered 2D arrangement is encountered in the $[Gd_4(btec)_3(H_2O)_{12}]\cdot 15H_2O$ [30] or $[Gd_4(btec)_3(H_2O)_{14}]\cdot 14H_2O$ [42] containing isolated monomeric $\{GdO_9\}$ or dimeric edge-sharing $\{Gd_2O_{16}\}$ units.

Instead of trapping water species, the lanthanide pyromellitate frameworks may also encapsulate N-donor organic moieties, which are usually observed under their protonated form, leading to the occurrence of ammonium groups. The latter balances the negative charges of the btec linker, resulting in a 1/1 ratio for the neutral network with typical $[Ln^{3+}(btec)^{4-}]\cdot R\text{-}N^+$ formula. These ammonium-based species may thus play the role of templating or structure-directing agents in order to create open-framework topologies with 3D nets arranged around them. This situation is reported in the lanthanide pyromellitates trapping cationic 4,4-bipyridinium (Pr, Eu, Gd),[43] azobipyridinium (Gd),[44] piperazinediium (Pr)[45] or formyldimethylammonium species (La)[46]. In other structures, the ammonium organic molecules are observed as intercalated species between layers of lanthanide-btec nets (for instance in $[Ln(btec(H_2O)_5]\cdot$4-aminopyridinium$\cdot 3H_2O$ (Ln = Eu [47] or Tb [48]).

Following this observation, the present study describes the solvothermal synthesis and characterization of two distinct structural topologies based on the assembly of trivalent lanthanides with pyromellitate ligand, involving the encapsulation of cationic dimethylammonium ($(CH_3)_2NH_2^+$) species. Indeed, depending on the choice of lanthanide elements, two crystal structures have been identified, related to light 4*f* cations (here La^{3+}, Ce^{3+}, Pr^{3+}) or heavy 4*f* cations (here Dy^{3+}, Yb^{3+}). The first series corresponds to the compounds $(CH_3)_2NH_2[Ln(btec)]\cdot 2H_2O$ (Ln = Ce (**1**), La (**2**), Pr (**3**)) with free water together with dimethylammonium species inserted within the cavities of the 3D network, whereas the second series concerns the compounds $(CH_3)_2NH_2[Ln(btec)(H_2O)]$ (Ln = Dy (**4**), Yb (**5**)) and exhibits a different 3D topology with encapsulated dimethylammonium species, but water molecule bonded to the lanthanide centers. In our chemical system, the dimethylammonium moieties came from the partial decomposition of the organic N,N-dimethylformamide used as co-solvent with water in our solvothermal synthesis route. In order to slow down the nucleation kinetic for promoting the crystal growth, we also used a modulator agent such as 2-fluorobenzoic acid.

The latter was previously known to control the crystalline growth in diverse rare-earth carboxylate MOF-like materials such as UiO-66 topology. [49–52]
The two types of structural arrangements (**1**-**3** & **4**,**5**) have been analyzed by single-crystal X-ray diffraction, and thermal investigations led to an unexpected single crystal to single crystal phase transition occurring during the dehydration process of the compounds of the series **1**-**3**, notably with the cerium-containing compound (**1**) leading to the dehydrated phase (**1'**). This structural change is discussed in term of atomic arrangement modification and indicates a significant flexibility of the 3D framework of **1**, which is related to a breathing effect and rarely observed in rare-earth coordination polymers. Tentative calculations were made to investigate the water sorption process.

Experimental Section

Reagents. The following reactants were used: ammonium cerium(IV) nitrate ($(NH_4)_2Ce(NO_3)_6$, 99%, Sigma-Aldrich), lanthanum(III) nitrate hexahydrate ($La(NO_3)_3{\cdot}6H_2O$, >99%, Fluka), praseodymium(III) nitrate hexahydrate ($Pr(NO_3)_3{\cdot}6H_2O$, 99.9%, Alpha Aesar), dysprosium(III) nitrate hexahydrate ($Dy(NO_3)_3{\cdot}6H_2O$, 99.99%, Alfa Aesar), ytterbium(III) nitrate hexahydrate ($Yb(NO_3)_3{\cdot}6H_2O$, 99.99%, Alfa Aesar), 1,2,4,5-benzenetetracarboxylic acid ($C_{10}H_6O_8$, known as pyromellitic acid, noted H_4btec, 99%, Sigma-Aldrich), 2-fluorobenzenecarboxylic acid ($C_7H_5FO_2$, 98%, Sigma-Aldrich), N,N-dimethylformamide (C_3H_7NO, noted DMF, 99.8%, Sigma-Aldrich). The chemical reactants were commercially available, were used without any further purification.

Syntheses

Compound **1** $(CH_3)_2NH_2[Ce(btec)]{\cdot}2H_2O$: A mixture of 164 mg (0.3mmol) $(NH_4)_2Ce(NO_3)_6$ with 76 mg (0.3 mmol) 1,2,4,5-benzenetetracarboxylic acid, 210 mg (1.5 mmol) of 2-fluorobenzoic acid, 3 mL (39 mmol) N,N-dimethylformamide and 3 mL (167 mmol) H_2O was placed in a 12 mL glass tube, sealed with a phenolic cap. The glass tube was then heated at 100°C for 72 hours. The resulting yellow crystals product was filtered off, washed with DMF solvent and finally dried at room temperature in air atmosphere. It was analyzed by optical and scanning electron microscope showing elongated parallelepiped-shape crystals of 200-400 μm size. Yield reaction was 61.8 % Ce. (Figure S1a). CHN elemental analysis has been performed by using the Elementar vario EL cube apparatus with sulfanilic acid as standard. It gives C: 29.2% (calc. 30.5%), H: 2.65% (calc. 2.97%) and N: 2.72 % (calc. 2.97%).

Compound **1'** $(CH_3)_2NH_2[Ce(btec)]$, was obtained from calcination of crystals of compound **1** at 120°C overnight under 3 mmHg vacuum.

Compound **2** $(CH_3)_2NH_2[La(btec)]{\cdot}2H_2O$: The procedure used for compound **1** synthesis was reproduced using a mixture of 130 mg (0.3 mmol) $La(NO_3)_3{\cdot}6H_2O$ with 76 mg (0.3 mmol) 1,2,4,5-benzenetetracarboxylic acid, 210 mg (1.5 mmol) of 2-fluorobenzoic acid, 3 mL (39 mmol) N,N-dimethylformamide and 3 mL (167 mmol) H_2O. The resulting colorless crystals obtained were analyzed by optical and scanning electron microscope showing elongated parallelepiped-shape crystals of 10-100 μm size (Figure S1b). Yield reaction was 65.8 % La.

CHN elemental analysis has been performed by using the Elementar vario EL cube apparatus with sulfanilic acid as standard. It gives C: 28.7% (calc. 30.6%), H: 2.81% (calc. 2.97%) and N: 2.70 % (calc. 2.97%).

Compound **3** $(CH_3)_2NH_2[Pr(btec)]\cdot 2H_2O$: The procedure used for compound **1** synthesis was reproduced using a mixture of 125 mg (0.29 mmol) $Pr(NO_3)_3\cdot 6H_2O$, 76 mg (0.3 mmol) 1,2,4,5-benzenetetracarboxylic acid, 210.2 mg (1.5 mmol) of 2-fluorobenzoic acid, 3 mL (39 mmol) N,N-dimethylformamide and 3 mL (167 mmol) H_2O. The resulting colorless crystals obtained were analyzed by optical and scanning electron microscope showing elongated parallelepiped-shape crystals of 100-500 μm size (Figure S1c). Yield reaction was 61.8 % Pr. CHN elemental analysis has been performed by using the Elementar vario EL cube apparatus with sulfanilic acid as standard. It gives C: 29.7% (calc. 30.4%), H: 3.03 % (calc. 2.96%) and N: 2.86 % (calc. 2.96%).

Compound **4** $(CH_3)_2NH_2[Dy(btec)(H_2O)]$: The procedure used for compound **1** synthesis was reproduced using a mixture of 132 mg (0.3 mmol) $Dy(NO_3)_3\cdot 5H_2O$, 76 mg (0.3 mmol) 1,2,4,5-benzenetetracarboxylic acid, 210 mg (1.5 mmol) of 2-fluorobenzoic acid, 3 mL (39 mmol) N,N-dimethylformamide and 3 mL (167 mmol) H_2O. The resulting colorless crystals obtained were analyzed by optical and scanning electron microscope showing elongated parallelepiped-shape crystals of 100-200 μm size (Figure S1d). Yield reaction was 57.3 % Dy. CHN elemental analysis has been performed by using the Elementar vario EL cube apparatus with sulfanilic acid as standard. It gives C: 29.6% (calc. 30.2%), H: 2.55% (calc. 2.52%) and N: 2.91 % (calc. 2.94%).

Compound **5** $(CH_3)_2NH_2[Yb(btec)(H_2O)]$: The procedure used for compound **1** synthesis was reproduced using a mixture of 135 mg (0.3 mmol) $Yb(NO_3)_3\cdot 5H_2O$ with 3 mM of H_2O, 76 mg (0.3 mmol) 1,2,4,5-benzenetetracarboxylic acid, 210 mg (1.5 mmol) of 2-fluorobenzoic acid, 3 mL (39 mmol) N,N-dimethylformamide and 3 mL (167 mmol) H_2O. The resulting colorless crystals obtained were analyzed by optical and scanning electron microscope showing elongated parallelepiped-shape crystals of 50-300 μm size (Figure S1e). Yield reaction was 58.5 %Yb. CHN elemental analysis has been performed by using the Elementar vario EL cube apparatus with sulfanilic acid as standard. It gives C: 28.8% (calc. 29.6%), H: 2.47% (calc. 2.46%) and N: 2.85 % (calc. 2.87%).

Single-crystal X-ray diffraction

Crystals of compounds **1**-**5** were selected under polarizing optical microscope and glued on a glass fiber for single-crystal X-ray diffraction experiments. X-ray intensity data were collected using a Bruker DUO-APEX2 CCD area-detector diffractometer using Mo-Kα radiation (λ = 0.71073 Å, for compounds **1**, **1'** and compounds **2**-**5**) with an optical fiber as collimator at 100K under nitrogen flux for compounds **2** and **3** and at room temperature for compounds **1**, **1'**, **4** and **5**. Several sets of narrow data frames (10s per frame for compounds **1**, **2**, **4** and **5** and, 25s per frame for compound **3**) were collected with ω scans. Data reduction was accomplished using

SAINT V8.34a. [53] The substantial redundancy in data allowed a semi-empirical absorption correction (SADABS V2014/5) to be applied, [54] based on multiple measurements of equivalent reflections. The structures were solved by direct methods, developed by successive difference Fourier syntheses, and refined by full-matrix least-squares on all data using SHELX program suites, implemented in the OLEX2 interface.[55]

The crystal data are given in Table 1. Supporting information is available in CIF format. CCDC numbers: 2513429 for **1**, 2513431 for **1'**, 2513432 for **2**, 2513430 for **3**, 2513433 for **4** and 2513434 for **5** contain the supplementary crystallographic data for this paper. These data can be obtained free of charge from The Cambridge Crystallographic Data Centre via www.ccdc.cam.ac.uk/data_request/cif.

Table 1: Crystal data and structure refinements for compounds 1-5.

	Compound 1 **Ce**	**Compound 1'** **Ce**	**Compound 2** **La**	**Compound 3** **Pr**	**Compound 4** **Dy**	**Compound 5** **Yb**
Formula	$C_{10}H_2CeNO_{10}$	$C_{12}H_{10}CeNO_8$	$C_{10}H_2LaO_8$	$C_{10}H_2O_8Pr$	$C_{12}H_{12}DyNO_9$	$C_{12}H_{12}YbNO_9$
Formula weight	436.25	436.33	389.03	423.03	476.73	487.27
Temperature/K	296	300	100	100	302	303
Crystal type	colorless needle	colorless block	colorless block	colorless block	colorless block	colorless block
Crystal size/mm	0.167 x 0.068 x 0.049	0.056 x 0.017 x 0.016	0.11 x 0.07 x 0.016	0.045 x 0.022 x 0.010	0.09 x 0.3 x 0.015	0.06 x 0.026 x 0.015
Crystal system	triclinic	orthorhombic	triclinic	triclinic	triclinic	triclinic
Space group	*P*-1	$P2_12_12_1$	*P*-1	*P*-1	*P*-1	*P*-1
a/Å	7.417(2)	7.445(3)	7.4500(3)	7.3785(3)	6.0450(2)	5.9979(4)
b/Å	10.294(3)	12.330(4)	10.3363(4)	10.2589(5)	9.2872(3)	9.2433(6)
c/Å	11.201(3)	15.294(5)	11.2253(4)	11.1861(4)	13.0880(3)	13.0047(8)
α/°	97.198(10)	90	100.433(1)	97.239(2)	100.407(1)	100.234(3)
β/°	106.368(9)	90	106.567(1)	106.2781)	98.753(1)	98.613(2)
γ°	110.018(9)	90	110.466(1)	109.752(2)	95.714(1)	96.073(3)
Volume/Å^3	747.3(4)	1403.9(8)	737.31(5)	741.79(5)	708.14(4)	694.99(8)
Z, $\rho_{calculated}$/g.cm^{-3}	2 / 1.939	4 / 2.064	2 / 1.752	2 / 1.894	2 / 2.236	2 / 2.328
μ/mm^{-1}	1.633	25.469	2.923	3.327	5.326	6.779
Θ range/°	2.38 - 20.63	4.61 – 59.88	2.21 – 30.585	1.96 – 30.56	2.25 – 30.54	2.26 – 30.66
Limiting indices	$-9 \le h \le 9$ $-12 \le k \le 12$ $-14 \le l \le 14$	$-7 \le h \le 8$ $-13 \le k \le 13$ $-16 \le l \le 16$	$-10 \le h \le 10$ $-14 \le k \le 14$ $-16 \le l \le 16$	$-10 \le h \le 10$ $-14 \le k \le 14$ $-15 \le l \le 15$	$-8 \le h \le 8$ $-13 \le k \le 13$ $-18 \le l \le 18$	$-8 \le h \le 8$ $-13 \le k \le 13$ $-18 \le l \le 18$
Collected reflections	9954	10084	72655	53092	52466	76344
Unique reflections	3082 [R(int) = 0.0684]	2000 [R(int) = 0.0981]	4527 [R(int) = 0.0407]	4544 [R(int) = 0.0518]	4339 [R(int) = 0.0451]	4305 [R(int) = 0.0518]
Parameters	192	201	172	200	226	211
Flack parameter	/	0.597(19)	/	/	/	/
Goodness-of-fit on F^2	1.106	1.053	1.110	1.109	1.137	1.149
Final R indices [I>2σ(I)]	R1 = 0.0421 wR2 = 0.1099	R1 = 0.0553 wR2 = 0.1299	R1 = 0.0420 wR2 = 0.1272	R1 = 0.0419 wR2 = 0.1203	R1 = 0.0177 wR2 = 0.0352	R1 = 0.0181 wR2 = 0.0347
R indices (all data)	R1 = 0.0495 wR2 = 0.1143	R1 = 0.0748 wR2 = 0.1391	R1 = 0.0445 wR2 = 0.1302	R1 = 0.0458 wR2 = 0.1235	R1 = 0.0216 wR2 = 0.0372	R1 = 0.0231 wR2 = 0.0368
Largest diff. peak and hole/e.Å^{-3}	1.465 and -1.382	1.102 and -1.852	6.245 and -0.872	5.265 and -1.357	0.717 and -0.769	0.716 and -0.923

Powder X-ray diffraction

X-ray powder diffraction was performed on Bruker D8 Advance diffractometer (LynxEye detector) in a Bragg-Brentano θ-θ mode using Cu-Kα radiation. Each powder pattern was recorded within an angular range of 5-50° in 2θ, with steps of 0.02° and counting time of 0.5 s per step.

Scanning electron microscopy

The SEM analyses of compounds 1-5 were performed on a Hitachi-S3400N microscope, equipped with a tungsten filament (acceleration voltage =3 kV, secondary electron mode, working distance = 5 to 10 mm). Images are given on part S1 microscopy in the supplementary informations.

Infrared spectroscopy

Infrared spectrum of compounds **1-5** were measured on Perkin Elmer Spectrum TwoTM spectrometer between 4000 and 400 cm^{-1}, equipped with a diamond Attenuated Total Reflectance (ATR) accessory. No ATR correction was applied on the spectrum. The Spectra can be found in the supplementary informations (Figure S4a and S4b and Table S4a).

Thermogravimetric analysis

Thermogravimetric curves (See supplementary informations section S3) have been collected on the thermo-analyzer 92 SETARAM TGA up to 800°C under air flow, with a heating rate of $5°C.min^{-1}$.

N_2 Surface Area and water adsorption measurements

N_2 sorption at liquid nitrogen temperature (N_2 bath at 77 K) and water sorption at 25°C (temperature set with a Micromeritics iso-controller bath) were realized in a Micromeritics Triflex apparatus using samples previously degassed under secondary vacuum at 120 °C. The multipoint BET (Brunauer−Emmett− Teller) model in the 0.02−0.3 p/p_0 range evaluated the specific surface area of the examined samples.

Molecular simulations

In order to probe the adsorption sites and simulate the adsorption isotherms, Grand Canonical Monte Carlo calculations have been performed using a home-made code. The initial step for the simulations was to optimize the experimental crystal structure by DFT using $DMol^3$ (BIOVIA)[56] and considering the functional GGA/PBE and the DNP basis set. The geometry optimization procedure was finished when the convergence was reached following the criteria: Quality fine; Energy variation $<10^{-5}$ Ha; Max. Force variation < 0.002 Ha/Å; Max displacement <0.005 Å. Then, using these DFT calculations, it was also possible to extract the partial charges for atoms using Mulliken analysis. The values for partial charges are reported in SI file (Figure S5b and table S5a). For the open form structure, 4 water molecules and guest extra-framework ions has been considered in the pores to build the initial structure in order to be consistent with experimental data.

The so-obtained structures were then used for Grand Canonical Monte Carlo (GCMC) calculations. Thus, water and Ce-MOF parameters were implemented in GCMC code (DFT partial charges to calculate the electrostatic interaction and Lennard-Jones parameters coming from UFF to evaluate the van der Waals interactions for both the framework and the extra-framework ion). The charges and the Lennard-Jones parameters for water molecules were taken from the TIP-4P-2005 force field.[57] The Ewald summation was used for electrostatic part of energy and a cut-off distance of 12 Å was applied for Lennard-Jones parameters. The calculations were performed with $2x10^7$ and $5x10^6$ Monte Carlo steps for equilibration and production, respectively. The simulations were conducted at 300 K using a multi-cell structure based on the optimized structures considered as rigid with 4x3x3 = 36 unit-cells for the open

form and 4x3x2 = 24 unit-cells for the closed form in order to be consistent with the 12 Å cut-off distance.
Using such a procedure, it was possible to determine the amount of water adsorbed as a function of the relative humidity so as to plot the adsorption isotherm. Furthermore, for a water loading fixed at 1 molecule/multi-cell, the enthalpy of water adsorption onto Ce-MOF was extracted from Monte Carlo simulations. The most stable configurations of water molecules in the pores of the solids were also identified on which to base the discussion about the plausible adsorption sites.
Additional parameters calculated from the structure included the pore volume and the specific surface area for N_2. The theoretical parameters could be compared with the experimental values. Following the strategy previously developed by Düren et al.,[58] the area defined by the motion of the center of a nitrogen molecule rolling along the surface allowed calculation of the specific surface area. The diameter of the probe molecule was considered to be equal to 3.681 Å, whereas the diameter of each atom constituting the MOF structure was taken from UFF force field. The pore volume was calculated using a similar method of trial insertions with the entire volume of the unit cell. A 0 Å-size probe was used for the determination of the free volume of the unit cell unoccupied by the framework atoms.

Results

Structure description of $(CH_3)_2NH_2[Ln(btec)]\cdot 2H_2O$ (Ln = Ce (1), La (2), Pr (3))
The compounds **1**, **2** and **3**, incorporating Ce(III), La(III) and Pr(III) respectively, are isostructural (see powder XRD patterns reported in Figure S2c). Their crystal structure ($(CH_3)_2NH_2[Ln(btec)]\cdot 2H_2O$) is built up from lanthanide atoms connected to each other through pyromellitate ligands, in order to generate a three-dimensional framework. For sake of clarity, only the cerium-containing phase is described; the atomic metrics of the La- and Pr-analogs are indicated in supplementary info (Table S2a) and follow the expected bond length contraction from La(III) to Pr(III) in the periodic table.
In compound **1**, the unique crystallographically independent cerium center is nine-fold coordinated in a distorted tricapped trigonal prismatic geometry with the oxygen atoms from carboxylate arms of the tetratopic linkers (Figure 1 – top). The Ce-O bond distances are in the expected range of 2.443(5)-2.680(4) Å, for such cerium(III) cation. The cerium-centered polyhedra [CeO_9] are linked to each other via edge-sharing mode (through two pairs of O3 and O7 oxygen atoms) with a *cis* sequence in order to generate corrugated infinite chains developed along the *a* axis (Figure 1 – bottom). The Ce⋯Ce distance within such $[CeO_9]_\infty$ rods is 4.0093(10) Å.

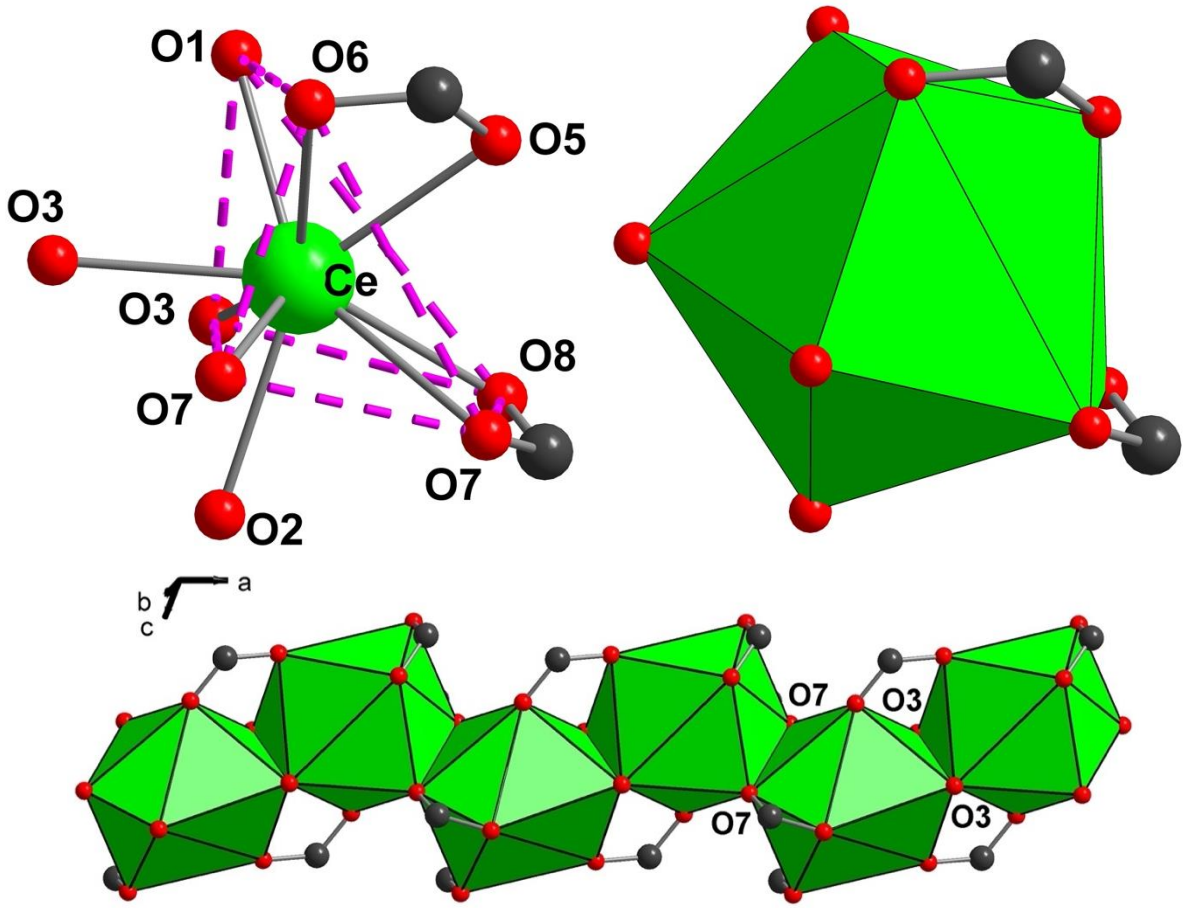

Figure 1: (top) Ball and Stick, and polyhedral representations of the distorted tricapped trigonal prismatic environment [LnO_9] of the unique cerium center in $(CH_3)_2NH_2$[Ln(btec)]·$2H_2O$ (Ln = Ce(**1**), La (**2**), Pr (**3**)). (bottom) Representation of the connection mode of the tricapped trigonal prismatic polyhedra generating infinite chains running along the *a* axis. Green circles or polyhedra: cerium; red circles: oxygen; dark grey circles: carbon.

While the unique cerium atom occupies a general position (2*i*), there are two inequivalent crystallographic pyromellitate linkers (called btec_A and btec_B), whose aromatic ring barycenters are located at around an inversion center (position 1*c* (0 ½ 0) for btec_A and position 1*b* (0 0 ½) for btec_B). Therefore, the two distinct organic tetratopic ligands count for half each in the resulting chemical formula of [Ce(btec_A)$_{0.5}$(btec_B)$_{0.5}$] network for compound **1**. Each pyromellitate molecule is linked to six cerium centers through the four carboxylates arms, but with different connection fashions (Figure 2). For the molecule btec_A, the two opposite carboxylate pincers adopt either a *syn-syn* bidentate bridging mode (through C1 carboxylate arm) with two adjacent cerium centers or chelating bridging mode (through C5 carboxylate arm) with one cerium center. The configuration of the second molecule (btec_B) differs with two carboxylate arms (through C6) in position 1,4 acting as monodentate mode with two adjacent cerium centers. The remaining C6-O4 bond remains free, with typical C=O distance of 1.227(9) Å. The two other opposite carboxylate arms (through C10) in position 2,5, adopt both chelating and *syn-anti* bidentate connection mode, with two adjacent cerium atoms.

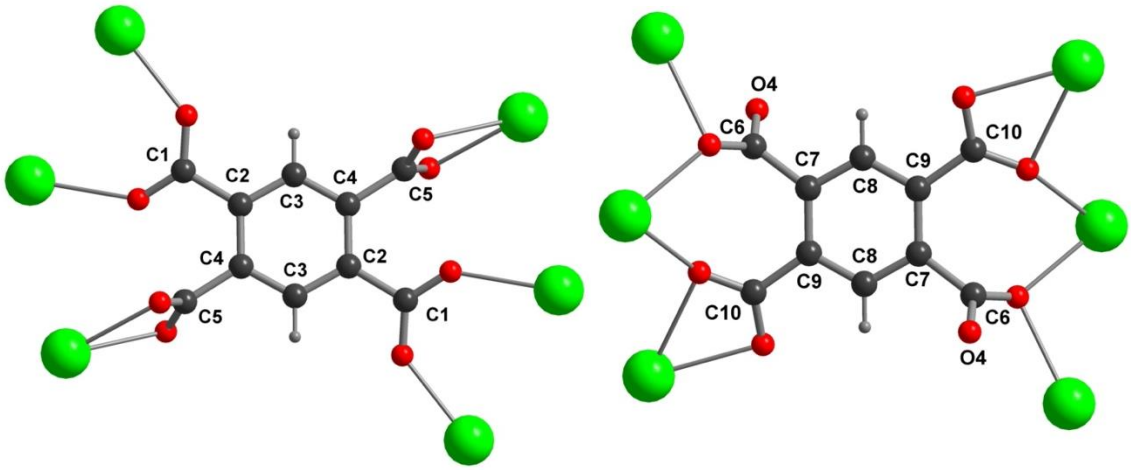

Figure 2: Representations of the connection modes of the two crystallographically inequivalent pyromellitate ligands (called btec_A – left and btec_B – right) in compounds **1,2,3**. Both organic molecules adopt a hexadentate bridging fashion with the cerium atoms, but the C6-O4 bond remains not shared with cerium centers with a distance of 1.227(9) Å (for the Ce compound **1**), related to a C=O bonding type. Green circles: cerium; red circles: oxygen; dark grey circles: carbon; light grey circles: hydrogen.

The connection of the infinite rods of [CeO_9] trigonal prisms with the two types of pyromellitates gives rise to the formation a three-dimensional network (Figure 3) in which the btec_A molecules are aligned along the *c* axis and the btec_B molecules are aligned along the *b* axis. It results in a framework delimiting one-dimensional lozenge-shape channels developed along the *a* axis of the inorganic chains of [CeO_9] polyhedra, with a free aperture size of around 4.2 x 8.2 $Å^2$ (based on the ionic radius of 1.35 Å for oxygen). It can be viewed as a square net with a distortion α angle of ≈97.2°, in which the $[CeO_9]_\infty$ rods correspond to the nodes linked to four neighboring ones through two sets of opposite hexadentate pyromellitate ligands along the *b* and *c* axes directions. This distortion is very similar in the case of praseodymium-analog, with a slightly decrease of the volume cell from 747.3(4) $Å^3$ down to 741.79(5) $Å^3$ as expected from the lanthanide contraction consideration. However, the use of larger lanthanide such as lanthanum gives rise to a more flattened network with the α angle of ≈100.4° (instead of ≈97.2°), resulting in the reduced cell volume of 737.31(5) $Å^3$.

This network topology belongs to the family of coordination polymers involving rod-packing systems, which has been described in many metal-organic frameworks solids,[59,60] corresponding to the *sra*-net of $SrAl_2$ type, [61] and reminds the structures of the MIL-53/47 series for instance.[62] It is also related to the similar crystal structures obtained with other lanthanides such as Pr(III), Eu(III), Gd(III) [43] with channels encapsulating 4,4'-bipyridinium cations or Gd(III) [44] with channels encapsulating 4,4'-azopyridinium cations. Indeed, the occurrence of trivalent lanthanides induces a negatively charged network $[Ln(btec)]^-$, due to the fully deprotonated tetratopic ligand, and it has to be compensated by trapped cationic species (pyridinium-derived molecules in the previous studies). In our case, the single-crystal X-ray diffraction analysis did however reveal a disordering situation with electronic densities randomly located within the rhombic channels, without observing well-defined molecules. The identification of the trapped species was carried out by means of further characterizations, involving thermogravimetric and chemical elementary analysis, as well as thermal transformation behavior (See below).

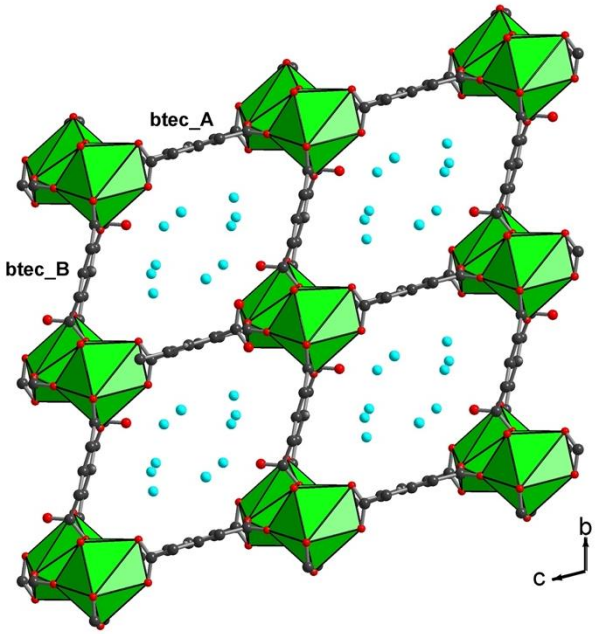

Figure 3: View of the structure of $(CH_3)_2NH_2[Ce(btec)]\cdot 2H_2O$ (**1**) showing the connection of the infinite chains of $[CeO_9]$ polyhedra linked to the two types of pyromellitate ligands, pyro_A along the *c* axis and pyro_B along the *b* axis. Lozenge-shaped tunnels developed along the *a* axis encapsulated water and dimethylammonium species, which cannot be localized by X-ray diffraction analysis due to atomic disorder (cyan circles related to the highest electronic densities). Green polyhedra: cerium; red circles: oxygen; dark grey circles: carbon.

Isolation of the thermally activated form of compound 1: $(CH_3)_2NH_2[Ce(btec)]$ (1')

In order to tentatively evacuate any possible solvent molecules (H_2O, DMF) trapped within the channels, compound **1** has been heated at 120°C overnight under vacuum and the resulting product has been further characterized by X-ray diffraction techniques. Its powder XRD pattern indicated a well-crystalline phase (named compound **1'**) drastically differs from the as-synthesized compound **1** (Figure S2a). The examination under the optical microscope still reveals well-shaped crystals which have been successfully used for single-crystal X-ray diffraction analysis.

Crystal structure of compound **1'** consists of the same arrangement of infinite chains of cerium-centered tricapped trigonal prims, linked through the pyromellitate ligands (Figure S2e). The cerium atom (siting on a general position 4*a*) is still coordinated with carboxyl oxygen atoms with eight Ce-O bond lengths in the typical range 2.444(13)-2.623(12) Å. Nevertheless, it is observed a ninth Ce-O2 bond with a much longer distance of 2.875(15) Å, which complete the nine-fold coordination, with a distorted trigonal tricapped trigonal prismatic geometry. The connection of the cerium-centered polyhedra $[CeO_9]$ through edge-sharing mode (with pairs of 'O3,O7' oxygen atoms) results in the formation of similar rods running along the *a* axis (Figure S2e), in which the Ce···Ce distance is 4.0976(14) Å. Whereas two distinct pyromellitate ligands (btec_A and btec_B) occur in compound **1**, there exists only one crystallographically independent organic linker in compound **1'** with a hexadentate connection mode towards the cerium centers and represents a mixture of the fashions observed from compound **1** (Figure 4). Indeed, the 1,2 carboxylate groups adopt either a chelating mode (through C1) or *syn-syn* bidentate bridging mode (through C8) as in btec_A. The second pair of carboxylate groups (in

4,5 position) exhibits either a monodentate mode, with a remaining unbonded C10-O4 linkage of 1.23(2) Å, corresponding to a C=O type, or a chelating and *syn-anti* bidentate connection mode, with two adjacent cerium atoms.

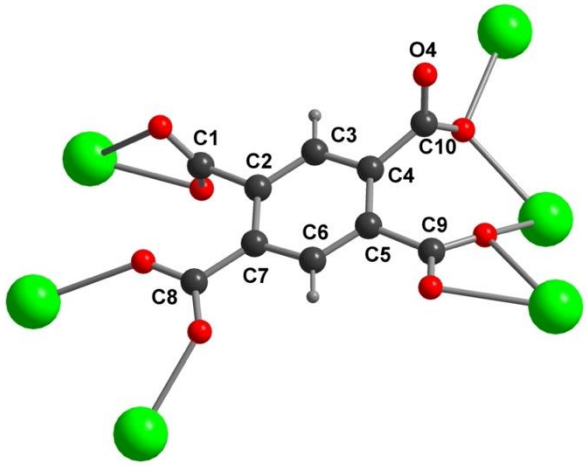

Figure 4: Representations of the connection mode towards cerium atoms of the unique crystallographically inequivalent pyromellitate ligand in compound **1'**. The C10-O4 bond remains not shared with cerium centers with a distance of 1.23(2) Å, related to a C=O bonding type. Green circles: cerium; red circles: oxygen; dark grey circles: carbon; light grey circles: hydrogen.

The assembly of the inorganic chains of [CeO_9] polyhedra connection of the infinite rods of [CeO_9] trigonal prisms with the pyromellitate linkers generates a three-dimensional network (Figure 5). It delimits one-dimensional distorted rectangular-shape channels developed along the *a* axis, with a free aperture size of around 4.3 x 7.2 $Å^2$ (based on the ionic radius of 1.35 Å for oxygen). Within the channels, it is clearly observed the presence of well-ordered cationic dimethylammonium species ($((CH_3)_2NH_2^+)$), revealing the decomposition of the N,N-dimethylformamide co-solvent under the hydrothermal conditions. Such a hydrolysis reaction is not surprising since it has been reported in many chemical systems involving the formation of metal-organic coordination polymers,[63] such as cerium- or uranyl-organic frameworks for instance.[64–66] The trapped organic molecule interacts through hydrogen bonds between the two protons of the ammonium group and oxygen atoms of the framework (N-H1B···O2 = 1.931(16) Å and N-H1A···O1 = 1.873(15) Å). The observation of such cationic species ensures the electroneutrality of the structure, with the consideration of the anionic cerium pyromellitate network $[Ce(btec)]^-$. Moreover, it gives the information about the nature of encapsulated molecules since the X-ray diffraction analysis of the as-synthesized compound (**1**) did not allow for a proper assignment.

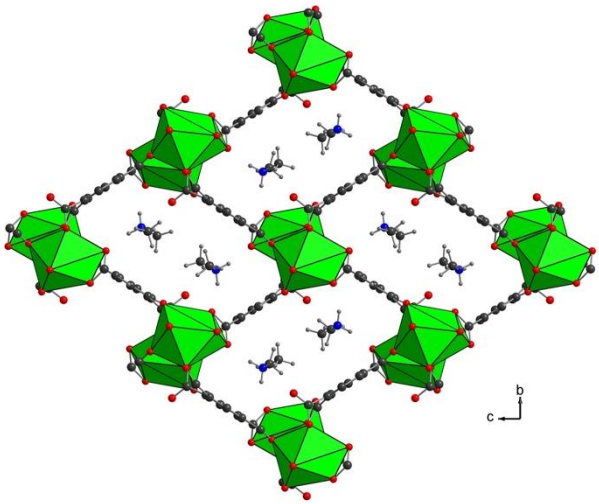

Figure 5: View of the structure of $(CH_3)_2NH_2[Ce(btec)]$ (**1'**) showing the connection of the infinite chains of $[CeO_9]$ polyhedra linked to the pyromellitate ligands along [011] and [0-11] directions. Distorted rectangular-shaped tunnels are developed along the *a* axis encapsulated dimethylammonium species. Green polyhedra: cerium; red circles: oxygen; dark grey circles: carbon; light grey circles: hydrogen.

Structure description of $(CH_3)_2NH_2[Ln(btec)(H_2O)]$ (Ln = Dy (4), Yb (5))

The structures of compounds **4** & **5** are similar (See Figure S2d) and differ from those of the series **1**-**3**, related to lighter lanthanides. They still consist of the connection of lanthanide centers (lying on general position 2*i*) with pyromellitate linkers, but the coordination environment displays an eight-fold $[DyO_8]$ or $[YbO_8]$ unit, in a distorted dicapped trigonal prismatic geometry (Figure 6). The unique crystallographically Dy or Yb atom is linked to seven oxygen atoms from carboxylate groups of the pyromellitate ligand, with Dy-O bond distances in the range 2.274(2)-2.492(2) Å (2.223(2)-2.457(2) Å for the Yb (**5**)). The coordination sphere is completed with an oxygen from a water species, with the bond lengths of Dy-OH_2 = 2.398(2) Å (label O1 on figure 6) and Yb-OH_2 = 2.349(2) Å (label O1). The $[DyO_7(H_2O)]$ or $[YbO_7(H_2O)]$ units are isolated from each other through two bidentate carboxylate groups, resulting in a secondary building brick composed of $[LnO_5(H_2O)\text{-}(OCO)_2\text{-}LnO_5(H_2O)]$ pairs of lanthanides (Figure 6). Within this brick, the interatomic distances between the closest lanthanide centers are 4.760(2) Å for Dy(4) and 4.723(5) Å Yb(5) indicating a longer spacing compared to those found in series **1**-**3** (≈ 4.4 Å), in which infinite ribbons of Ln-O-Ln sequence were observed.

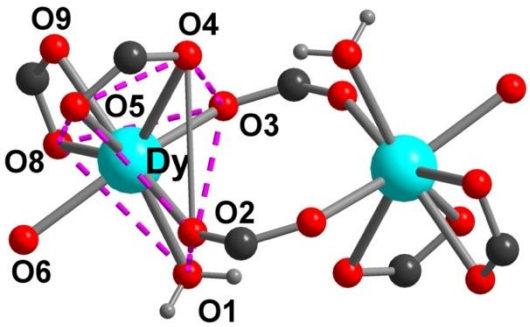

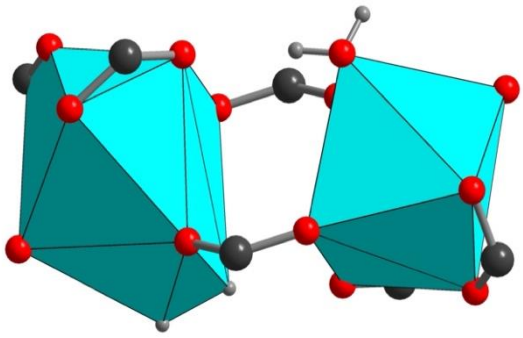

Figure 6: (top) Ball and Stick (top), and polyhedral (bottom) representations of the distorted dicapped trigonal prismatic environment [DyO_8] of the unique dysprosium center in $(CH_3)_2NH_2$[Dy(btec)(H_2O)] (**4**) and displaying the connection modes of the two [DyO_8] units through two carboxylate groups. Cyan circles or polyhedra: dysprosium; red circles: oxygen; dark grey circles: carbon; light grey circles: hydrogen.

As found in compounds **1-3**, one observes two inequivalent crystallographic pyromellitate linkers (called btec_A and btec_B; Figure 7), whose aromatic ring barycenters are located at around an inversion center (position 1*h* (½ ½ ½) for btec_A and position 1*d* (½ 0 0) for btec_B). Therefore, the two distinct organic tetratopic ligands count for half each in the resulting chemical formula of [(Dy/Yb)(btec_A)$_{0.5}$(btec_B)$_{0.5}$(H_2O)] network for compounds **4-5**. Each pyromellitate ligand adopts a different coordination scheme with the lanthanide centers: btec_A adopts a tetradentate connection mode with two opposite carboxylate arms (C5) in position 1,4, acting as a chelating fashion, and the two other carboxylate arms (C1) in position 2,5, are monodentate, remaining free one C=O bond with typical short length of 1.235(3) Å (for Dy (**4**)) and 1.239(3) Å (for Yb (**5**)). The second pyromellitate (btec_B) species is identical to that found for btec_A in series **1-3**, with the connection to six lanthanide centers: two of the opposite carboxylate arms (through C9) act as chelate, whereas the two others (through C6) are in a bidentate *syn-syn* configuration, bridging two neighboring lanthanide centers (Figure 7).

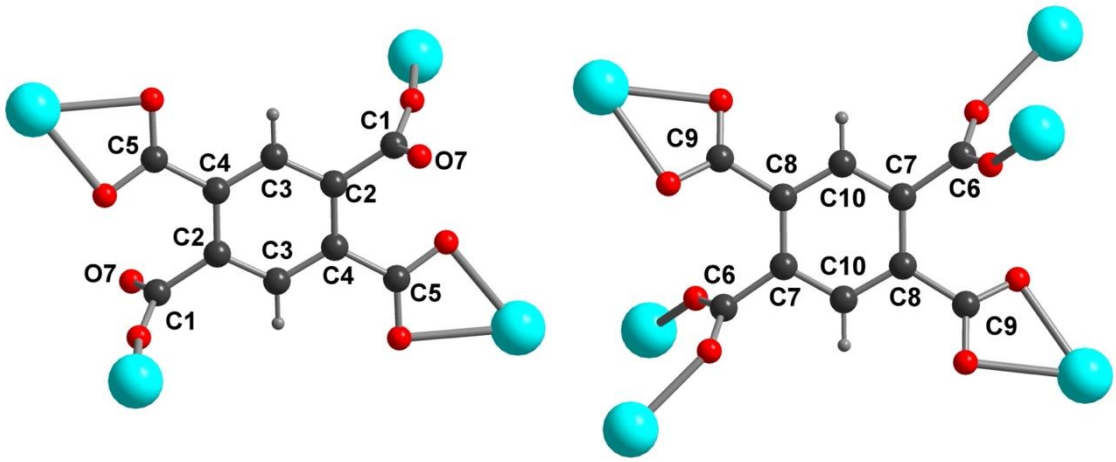

Figure 7: Representations of the connection modes of the two crystallographically inequivalent pyromellitate ligands (called btec_A – left and btec_B – right) in compounds **4, 5**. The organic molecule btec_A adopts a tetradentate bridging while the btec_B has a hexadentate bridging fashion with the dysprosium or ytterbium atoms. For btec_A, the C1-O7 bond remains unshared with lanthanide centers and is related to a C=O bonding type. Cyan circles: dysprosium or ytterbium; red circles: oxygen; dark grey circles: carbon; light grey circles: hydrogen.

The connection of the [$LnO_5(H_2O)$-$(OCO)_2$-$LnO_5(H_2O)$] dimers of lanthanides with the two types of pyromellitates results in the construction of a three-dimensional network (Figure 8) exhibiting one-dimensional flattened lozenge-shape channels developed along the *a* axis. When regarding the structure along the [100] direction, the btec_A molecules are aligned along the *c* axis, whereas the btec_B molecules are aligned along the *b* axis, both delimiting the tunnels. Its free aperture longest distance can be estimated at around 9 Å (based on the C-H closest groups along the *c* axis), but the occurrence of the unbonded C=O groups obstructs the channels along the [011] direction (C=O···O=C distance of 2.967(3) Å) in the middle. Indeed, two pockets are observed, in either side of the C=O···O=C axis. In each side pockets, they are well-ordered cationic dimethylammonium species ($(CH_3)_2NH_2^+$) which should also be found in the series **1**-**3**. These molecules show preferential hydrogen bond interactions between the protons of ammonium groups and oxygen atom from the terminal C=O bond (N1-H1C···O7 = 1.96(4) Å) and also oxygen atoms attached to the Dy or Yb center, via N1-H1D···O5 = 2.13(5) Å and N1-H1D···O5 = 2.45(4) Å).

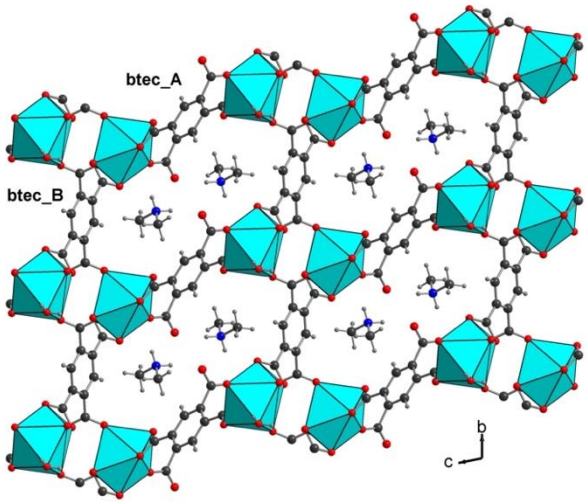

Figure 8: View of the structure of $(CH_3)_2NH_2$[Dy(btec)(H_2O)] (**4, 5**) showing the connection of the pairs of [DyO_8] polyhedra linked to the distinct pyromellitate ligands along the [001] direction. Distorted flattened rectangular-shaped tunnels are developed along the *a* axis encapsulated dimethylammonium species. Cyan polyhedra: cerium; red circles: oxygen; dark grey circles: carbon.

The structural arrangement of compounds **4**-**5** was found to be similar to that reported with the yttrium(III) in the CTH-14 solid,[44] which possesses the same 1D-tunnel topology of metallic dimeric entities, and encapsulating the same guest dimethylammonium species. This was described as by these authors. The occurrence of such similar crystal structures described as a *scu*-net, shows the expected and same chemical behavior for the yttrium as a 4*d* transition metal and the heavy trivalent 4*f* lanthanides such as dysprosium or ytterbium.

Thermal behavior study of the $(CH_3)_2NH_2$[Ce(btec)]·$2H_2O$ (1)

The as-synthesized powdered sample of the cerium pyromellitate **1** has been characterized by thermogravimetric analysis (Figure S3a) between room temperature and 800°C under air atmosphere. A first weight loss is observed up to 110°C, with a value of 8.0 %, which is assigned to the departure of water molecules, related to the ratio of 2 H_2O per [Ce(btec)] unit

(calculated: 7.6%). It is followed by a plateau up to ≈300°C, and then by a second event of weight loss up to ≈450°C. The remaining weight value is 37.3%, and attributed to the formation of CeO_2 (calculated: 36.4%; PDF file 01-075-0151).

This second loss includes the removal of the pyromellitate and dimethylammonium species, which results in the structure collapse of compound **1**. From this analysis, compound **1** is considered as a double hydrated form of cerium pyromellitate $(CH_3)_2NH_2[Ce(btec)]\cdot 2H_2O$, since the water molecules are not observed in the thermally activated compound **1'** with the chemical formula $(CH_3)_2NH_2[Ce(btec)]$. Elementary chemical analysis is in good agreement with the formula $(CH_3)_2NH_2[Ce(btec)]\cdot 2H_2O$ for compound **1** (see synthesis part). In addition, A squeeze procedure using PLATON software was applied to check the attribution of the molecules within the pores of compounds **1** (Table S3). A good correlation corresponding to 2 water molecules and one dimethylammonium cation was found. The compound **1** has been analyzed by use of thermal X-ray diffraction technique. The powder X-ray diffraction patterns have been measured as a function of temperature in the range 20-240°C (Figure S2b). One observes that Bragg peaks of compound **1** persist up to 60 °C. Above this temperature, the Bragg peaks of compound **1** start to disappear to the benefit of new Bragg peaks, indicating a phase transition into a new crystalline structure: compound **1'** (peaks at 9.2° and 11.5° (2θ)).

From both thermogravimetric and single-crystal X-ray diffraction analyses, it is deduced that the double hydrated cerium pyromellitate (**1**) can undergo a dehydration process starting at a temperature below 100°C without destructing the cerium pyromellitate network, and keeping the single-crystal integrity. Indeed, the hydrated form (**1**) delimits an achiral channel-like structure (*P*-1) with lozenge-shape encapsulating both dimethylammonium and water species. The dehydrated form (**1'**) only contains the dimethylammonium ones within the distorted rectangular-shape tunnels related to a chiral structure ($P2_12_12_1$). A slight transformation of the network is thus observed with the decrease of the cell volume ΔV of -6% from compound **1** (open form, V = 747.3(4) Å^3 with Z =2) to compound **1'** (closed form, V = 702.0(8) Å^3 for Z = 2) upon the evacuation of trapped water molecules. Such a cerium pyromellitate shows a certain structural flexibility since channel size is able to adapt with the steric hindrance of the encapsulated moieties. Indeed, the two previous lanthanide pyromellitates reported in literature indicate the trapping of either 4,4'-bipyridinium cations related to the cell volume V = 680.9 Å^3 (with Z =2, for the Gd(III)-member) and V = 712.7 Å^3 (with Z=2, for the Pr(III)-member)[43] or 4,4'-azopyridinium cations to the cell volume V = 735.4 Å^3 (with Z =2, for the Gd(III)-member).[44] Between these two gadolinium-containing pyromellitates, the variation of the cell volume values is ±7%. The aforementioned unit cells volumes appear greater in both cases than the reported volume of the dehydrated compound **1'** unit cell. In our study, the departure of water gives rise to the shrinkage of the framework together with the change of the tilting angle of the Ce···Ce axis (related to the shortest Ce···Ce interaction bonds, that are 4.0093(10) Å in **1** or 4.0976(14) Å in **1'**). The Ce···Ce axes are all orientated in the same direction of the achiral net (**1**) with a value of -16.41(6)° (Figure 9). But a rotation of the Ce···Ce axes is observed upon the shrinkage of the framework in compound **1'** with the alternation of ± 43.05(6)°, resulting in a chiral structure. This single-crystal to single-crystal transformation from one 3D net to a parent 3D' one has been well documented in literature,[67,68] but constitutes an unique example for the lanthanide pyromellitate case. Moreover, this structural modification with cell volume

variation is also reminiscent of a well-known property encountered in some MOF compounds, which may exhibit a reversible framework "breathing" phenomenon under external stimuli.[69,70] The best illustration is shown in the flexible networks such as MIL-53 or MIL-88,[62,71] with volume cell changes up to 47% or 85%, respectively. In these two examples, the volume cell changes are more important than in compound **1** as their cavities are free from any counter cations limiting the breathing process.

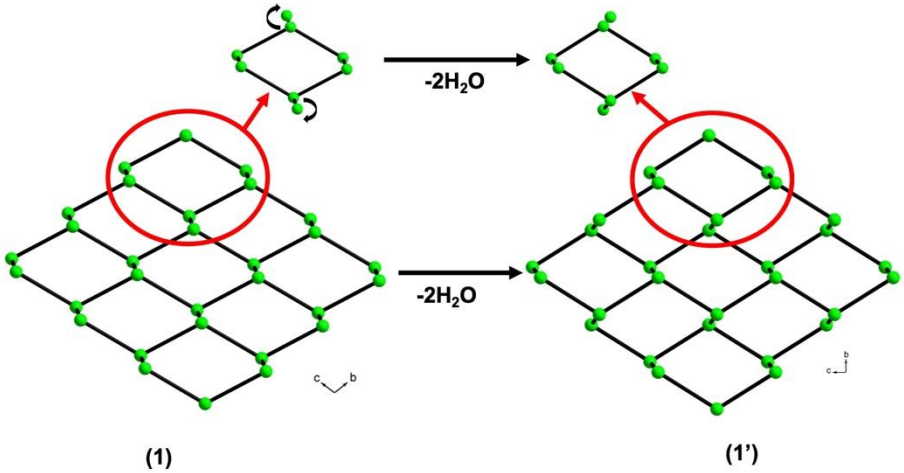

Figure 9: Schematic representation of the cerium centers (green circles) connectivity in the compound **1** network (open form, left) and its transformation upon water removal, resulting in network of compound **1'** (closed form, right). The departure of encapsulated trapped H_2O species induces the slight rotation of the Ce···Ce axis from tilting angle -16.41(6)° to + 43.05(6)°.

Thermal gravimetric analysis of compounds 2-5

The thermal behavior of compounds **2-5** has been characterized by thermogravimetric analyses under air atmosphere. For the isostructural series **1-3**, the experiment (Figures S3a-c) shows a first weight loss event up to 100°C, related to the departure of the two water molecules encapsulated within the channels (for **2**, obs.: 7.5 %; calc.: 7.6%; for **3**, obs.: 7.0 %; calc.: 7.6%). It is followed by a plateau up to 300 °C (**2**) or 320 °C (**3**), and then a large weight loss corresponding the degradation of the organic linkers and dimethylammonium cations together with the collapse of the three-dimensional structure, leading to the formation of La_2O_3 or Pr_2O_3 oxides from 690°C for (**2**; obs.: 36.0 %; calc.: 34.6%) or 490°C for (**3**; obs.: 36.9 %; calc.: 34.9%;). However, one observes one third transient event for the lanthanum-based compound, between 500 and 690°C, with a plateau (Figure S3b), which could be assigned to the formation of the intermediate as mixed lanthanum-oxide-carbonate ($La_2O_2CO_3$). This phase was reported to be stable in the range 450-730°C, during the decomposition of $La(CO_3)_3$ under air.[72] The decomposition of such $La_2O_2CO_3$ into La_2O_3 corresponds to the release of 1 CO_2 (calc.: 4.7 %), which is in very good agreement with the experimental weight loss value (5.1 %) observed between 500 and 690°C. For compounds 2 and 3, the squeeze procedure using PLATON software also give a good correlation corresponding to 2 water molecules and one dimethylammonium located inside the ores of the MOFs (Table S3). At the opposite, the compounds of series **4-5** do not exhibit any free trapped water species, but only water ligand attached to the lanthanide center. Indeed, the thermogravimetric curves (Figure S3c) still show a two-step weight loss event, with the departure of water followed by the removal of the organic

part, with the formation of final lanthanide oxides Dy_2O_3 (**4**; obs.: 36.9 %; calc.: 34.9%) or Yb_2O_3 (**5**; obs.: 36.9 %; calc.: 34.9 %). The removal of attached water species is shifted from room temperature for **1**-**3** up to 220 °C for both compounds **4** and **5**, with the expected weight losses of 1 H_2O per Ln unit (**4**, obs.: 4.7 %; calc.: 3.8 %; **5**, obs.: 4.4 %; calc.: 3.7 %).

Study of the adsorption of water in flexible compound 1'.

Before studying the water sorption on compound **1'**, we performed N_2 adsorption measurements to evaluate its specific surface area. It does not show any nitrogen adsorption, with a very low value of 0.00064 $cm^3.g^{-1}$, related to a surface area of around 0.24 $m^2.g^{-1}$. These experimental results are in concordance with the theoretical results for the closed form (dehydrated) for which no specific surface area is measured when N_2 is the probe and a pore volume is estimated at 0.14 $cm^3.g^{-1}$. For the open form (hydrated), the theoretical pore volume is calculated at 0.16 $cm^3.g^{-1}$. The water sorption of the anhydrous phase **1'** has been investigated in order to analyze the water uptake reversibility.

The isotherm curve of the adsorption of water (Figure 10) shows an unexpected two-steps event with a first uptake corresponding to the trapping of one H_2O molecule per $(CH_3)_2NH_2[Ce(btec)]$ unit (related to a transient stage $(CH_3)_2NH_2[Ce(btec)]\cdot H_2O$ up to p/p_0 at around 0.45, followed by the encapsulation of a second H_2O molecule, resulting in the dihydrated form, $(CH_3)_2NH_2[Ce(btec)]\cdot 2H_2O$, as initially observed in the as-synthesized compound **1**. When desorbing water, it is observed a hysteresis behavior, with the departure in one single step at low pressure (p/p_0 at around 0.15-0.1), as we found from the TG curve experiment. In addition, a second cycle of adsorption-desorption was also performed without significant degradation of the framework (Figure S6).

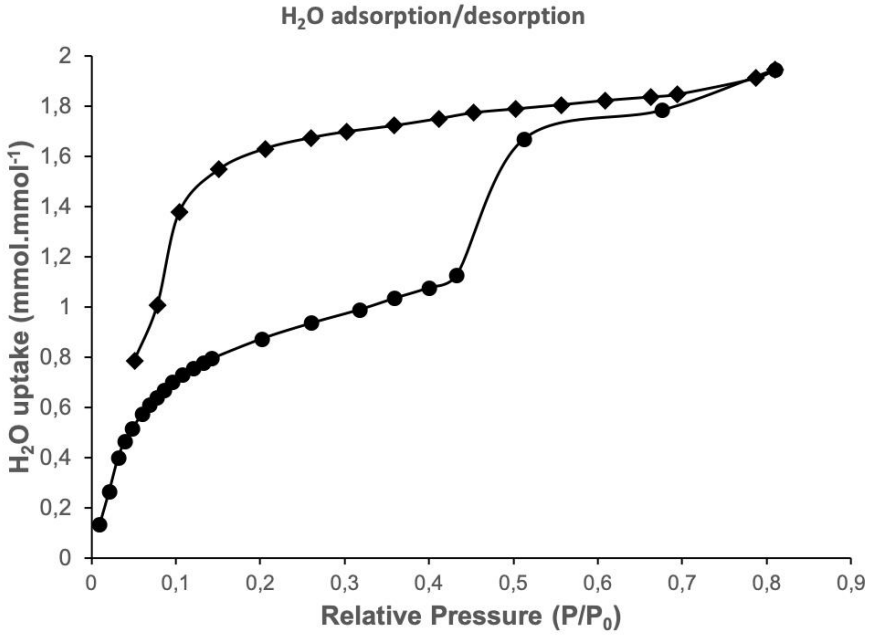

Figure 10: Isotherm curves of water vapor adsorption/desorption of compound **1'** ($(CH_3)_2NH_2[Ce(btec)]$) at 25°C. black circles: water adsorption ; black squares: desorption.

Using GCMC calculations, it is possible to model the adsorption isotherms for water in the open-form and closed form for Ce-MOF (corresponding to **1** and **1'** solids respectively) following the procedure described in Materials and Methods. For these calculations, the framework of the Ce-MOF and the dimethylammonium cations located within the pores were considered at the initial stage. The results are given in Figure 11.

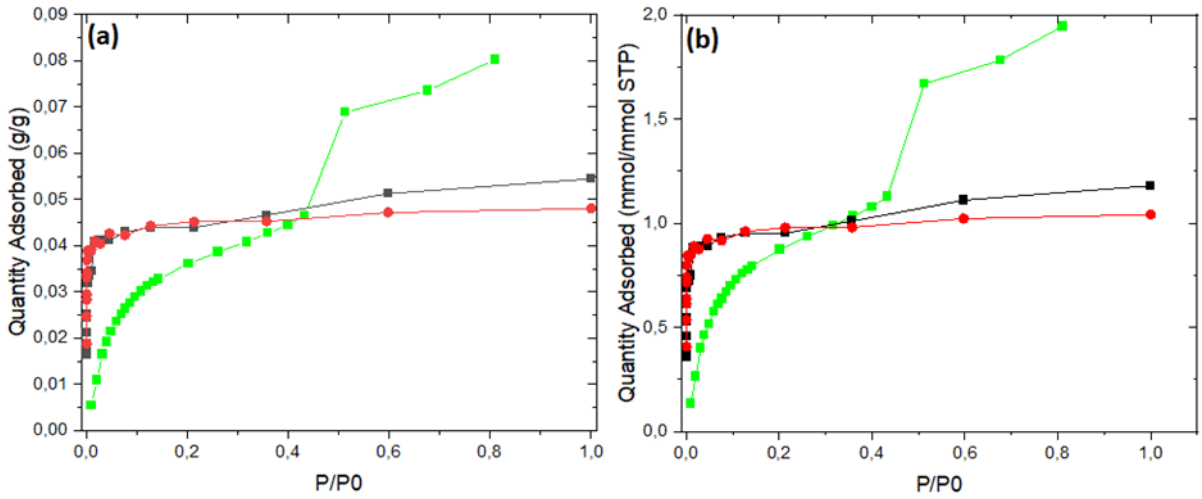

Figure 11: Theoretical Isotherms for open-form (black) and closed-form (red) for Ce-MOFs corresponding to experimental **1** and **1'** solids, obtained from GCMC calculations and given in g/g (a) and in mmol/mmol of Ce (b). The green curve corresponds to experimental data.

Based on the theoretical results, a strong affinity for water is observed for both open and closed-forms of Ce-MOF. Indeed, a deep increase of the water amount is obtained since the low relative humidity to reach a plateau close to 45 $mg.g^{-1}$ or 1 H_2O/mol of Ce. This plateau is in good agreement with the experimental inflexion point measured at p/p_0 = 0.45. This strong hydrophilicity is also in agreement with the adsorption enthalpy values calculated for both forms (~ 90-95 kJ/mol). However, GCMC calculations fail to reproduce the second step of the experimental adsorption isotherm to reach a water saturation close to 2 H_2O/Ce. Indeed, the theoretical saturation reached in the open-form is closed to 1.18 H_2O/Ce (to be compared with the saturation in closed-form evaluated at 1.04 H_2O/Ce). Anyway, molecular simulations show that the structural transition should occur due to the saturation of the pore volume of the closed-form of the Ce-MOF (**1'**), which requires to increase the volume to accommodate more water molecules.

To elucidate the water adsorption mechanism, configurations extracted from the GCMC calculations were analyzed and the snapshots are reported in Figure S5a.
As observed on the snapshots from the Figure S5a, the main interaction sites are the oxygen atoms from the framework which are in strong interaction with water molecules (distances between 1.6-2.0 Å for open-form and 2.0 and 2.4 Å for closed-form) while the distances between DMA^+ and framework are larger (>2.3Å). These small distances for water-framework are in good agreement with the theoretical adsorption enthalpies and the shape of the adsorption isotherms.

Furthermore, the modification of the structure could be explained by the sharing of some adsorption sites by both water and DMA^+, requiring the torsion of the ligand to accommodate both water and extra-framework cations.

Conclusion

In this contribution, we have synthesized and structurally analyzed five lanthanide-containing MOFs constructed by the association of pyromellitate ligands with Ce^{3+}, La^{3+}, Pr^{3+}, Dy^{3+} and Yb^{3+} cations. The five coordination polymers were solvothermally prepared in water/DMF solutions at 100°C and present two different structural organizations (one for Ce^{3+}, La^{3+} and Pr^{3+} and a second one for Dy^{3+} an Yb^{3+}). In both cases, the negative charge of the [LnBTEC] framework is compensated by the presence of one $[NH_2(CH_3)_2]^+$ cation located inside the cavities of the 3D network. In addition, the first structural organization with lighter lanthanides (compounds **1**-**3**) bears two water molecules within its cavities whereas the second one exhibits only one water molecule coordinated to the heavier lanthanide centers (compounds **4**-**5**). The dehydration process, below 100°C, occurs in the first structural type (**1**) without observing the collapse of the network, and keeping the structural integrity of the single crystals. This process causes the transition of an achiral lozenge shaped channel like structure (*P*-1) to a distorted rectangular shape chiral structure ($P2_12_12_1$) and a cell volume reduction of about 6%. It is also reversible and the dehydrated crystals can be rehydrated by absorption of 80 mg of water by g of MOF, closely corresponding to two water molecules per asymmetric units. It indicates a reversible breathing phenomenon for the first structural phase that has never been reported before for such Ln^{3+}-MOFs with pyromellitate ligands.

Supporting information

Optical and scanning electron microscopy photographs, PXRD patterns, tables of interatomic distances, TGA and IR spectroscopy of compounds **1-5** are given in the supplementary information file. Structural highlight on compound **2**, thermodiffraction of compound **1**, and additional informations on molecular simulations can also be found here.

Acknowledgments

The authors would like to thank Mrs Laurence Burylo, Mr Philippe Devaux, Mrs Celine Delabre and Mr Alejandro Vieyra Huerta for their assistances with the preliminary synthesis, XRD powder patterns measurements (UCCS) and elemental analyses measurements (UCCS). The "Fonds Européen de Développement Régional (FEDER)", "CNRS", "Région Hauts de France" and "Ministère de l'Education Nationale de l'Enseignement Supérieur et de la Recherche" are acknowledged for the funding of X-ray diffractometers from the Chevreul Institute platform.

References

(1) Zhou, H.-C.; Long, J. R.; Yaghi, O. M. Introduction to Metal–Organic Frameworks. *Chem. Rev.* **2012**, *112* (2), 673–674. https://doi.org/10.1021/cr300014x.

(2) Furukawa, H.; Cordova, K. E.; O'Keeffe, M.; Yaghi, O. M. The Chemistry and Applications of Metal-Organic Frameworks. *Science* **2013**, *341* (6149), 1230444. https://doi.org/10.1126/science.1230444.

(3) Zhou, H.-C. "Joe"; Kitagawa, S. Metal–Organic Frameworks (MOFs). *Chem. Soc. Rev.* **2014**, *43* (16), 5415–5418. https://doi.org/10.1039/C4CS90059F.

(4) Zhang, X.; Chen, Z.; Liu, X.; Hanna, S. L.; Wang, X.; Taheri-Ledari, R.; Maleki, A.; Li, P.; Farha, O. K. A Historical Overview of the Activation and Porosity of Metal–Organic Frameworks. *Chem. Soc. Rev.* **2020**, *49* (20), 7406–7427. https://doi.org/10.1039/D0CS00997K.

(5) Allendorf, M. D.; Bauer, C. A.; Bhakta, R. K.; Houk, R. J. T. Luminescent Metal–Organic Frameworks. *Chem. Soc. Rev.* **2009**, *38* (5), 1330. https://doi.org/10.1039/b802352m.

(6) Rocha, J.; Carlos, L. D.; Paz, F. A. A.; Ananias, D. Luminescent Multifunctional Lanthanides-Based Metal–Organic Frameworks. *Chem. Soc. Rev.* **2011**, *40* (2), 926–940. https://doi.org/10.1039/C0CS00130A.

(7) Cui, Y.; Yue, Y.; Qian, G.; Chen, B. Luminescent Functional Metal–Organic Frameworks. *Chem. Rev.* **2012**, *112* (2), 1126–1162. https://doi.org/10.1021/cr200101d.

(8) Yan, B. Lanthanide-Functionalized Metal–Organic Framework Hybrid Systems To Create Multiple Luminescent Centers for Chemical Sensing. *Acc. Chem. Res.* **2017**, *50* (11), 2789–2798. https://doi.org/10.1021/acs.accounts.7b00387.

(9) Roy, S.; Chakraborty, A.; Maji, T. K. Lanthanide–Organic Frameworks for Gas Storage and as Magneto-Luminescent Materials. *Coord. Chem. Rev.* **2014**, *273–274*, 139–164. https://doi.org/10.1016/j.ccr.2014.03.035.

(10) Pagis, C.; Ferbinteanu, M.; Rothenberg, G.; Tanase, S. Lanthanide-Based Metal Organic Frameworks: Synthetic Strategies and Catalytic Applications. *ACS Catal.* **2016**, *6* (9), 6063–6072. https://doi.org/10.1021/acscatal.6b01935.

(11) Zhang, Y.; Liu, S.; Zhao, Z.-S.; Wang, Z.; Zhang, R.; Liu, L.; Han, Z.-B. Recent Progress in Lanthanide Metal–Organic Frameworks and Their Derivatives in Catalytic Applications. *Inorg. Chem. Front.* **2021**, *8* (3), 590–619. https://doi.org/10.1039/D0QI01191F.

(12) Ghasempour, H.; Wang, K.-Y.; Powell, J. A.; ZareKarizi, F.; Lv, X.-L.; Morsali, A.; Zhou, H.-C. Metal–Organic Frameworks Based on Multicarboxylate Linkers. *Coord. Chem. Rev.* **2021**, *426*, 213542. https://doi.org/10.1016/j.ccr.2020.213542.

(13) Song, X.; Zhang, Y.; Sun, P.; Gao, J.; Shi, F. Lithium–Lanthanide Bimetallic Metal–Organic Frameworks towards Negative Electrode Materials for Lithium-Ion Batteries. *Chem. Eur. J.* **2020**, *26* (25), 5654–5661. https://doi.org/10.1002/chem.201904913.

(14) Amiaud, T.; Stephant, N.; Dessapt, R.; Serier-Brault, H. Microwave-Assisted Synthesis of Anhydrous Lanthanide-Based Coordination Polymers Built upon Benzene-1,2,4,5-Tetracarboxylic Acid. *Polyhedron* **2021**, *204*, 115261. https://doi.org/10.1016/j.poly.2021.115261.

(15) Bo, Q. B.; Sun, Z. X.; Sheng, Y. L.; Zhang, Z. W.; Sun, G. X.; Chen, C. L.; Li, Y. X. A Novel Boat-Shaped Rare Earth Complex with a 3-D Interlinked Structure of Pr(III) and 1,2,4,5-Benzenetetracarboxylic Acid. *J. Inorg. Organomet. Polym.* **2006**, *16* (3), 241–248. https://doi.org/10.1007/s10904-006-9046-7.

(16) Júnior, J. C. A.; Dos Santos, G. L.; Colaço, M. V.; Barroso, R. C.; Ferreira, F. F.; Dos Santos, M. V.; De Campos, N. R.; Marinho, M. V.; Jesus, L. T.; Freire, R. O.; Marques, L. F. New Eu ^{III} Pyromellitic Metal–Organic Framework of Intense Red-Orange

Luminescence and High Thermal Stability for Marking in Gunshot Residues. *J. Phys. Chem. C* **2020**, *124* (18), 9996–10006. https://doi.org/10.1021/acs.jpcc.0c01374.
(17) Sun, D.; Cao, R.; Liang, Y.; Shi, Q.; Hong, M. Syntheses, Crystal Structures and Properties of Two Novel Lanthanide–Carboxylate Polymeric Complexes. *J. Chem. Soc., Dalton Trans.* **2002**, No. 8, 1847–1851. https://doi.org/10.1039/b109985j.
(18) Silva, M. A.; De Campos, N. R.; Ferreira, L. A.; Flores, L. S.; Júnior, J. C. A.; Dos Santos, G. L.; Corrêa, C. C.; Dos Santos, T. C.; Ronconi, C. M.; Colaço, M. V.; Simões, T. R. G.; Marques, L. F.; Marinho, M. V. A New Photoluminescent Terbium(III) Coordination Network Constructed from 1,2,4,5-Benzenetetracarboxylic Acid: Synthesis, Structural Characterization and Application as a Potential Marker for Gunshot Residues. *Inorg. Chim. Acta* **2019**, *495*, 118967. https://doi.org/10.1016/j.ica.2019.118967.
(19) Dao-Feng, S.; Wen-Hua, B.; Rong, C.; Xing, L.; Qian, S.; Mao-Chun, H. Hydrothermal Synthesis and Structure of a New 3D Lanthanide-Carboxylate Framework, $[La(Btec)_{1/2}(H_2Btec)_{1/2}(H_2O)]_n$ (H_4Btec = 1,2,4,5-Benzenetetracarboxylic Acid). *Chin. J. Chem.* **2003**, *21* (4), 405–408. https://doi.org/10.1002/cjoc.20030210411.
(20) Wen, Y.-H.; Zhang, J.; Li, Z.-J.; Qin, Y.-Y.; Kang, Y.; Hu, R.-F.; Cheng, J.-K.; Yao, Y.-G. Poly[Diaqua(μ_6-Benzene-1,2,4,5-Tetracarboxylato)(μ_6-2,5-Dicarboxybenzene-1,4-Dicarboxylato)Dilanthanum(III)]. *Acta Crystallogr. E Struct. Rep. Online* **2004**, *60* (5), m535–m537. https://doi.org/10.1107/S1600536804007779.
(21) Yaghi, O. M.; Li, H.; Groy, T. L. Crystal Structure of 1,2,4,5-Benzenetetracarboxylate Monohydrate Cerium(III), C10H4CeO9. *Z. Kristallogr. NCS* **1997**, *212* (1), 457–458. https://doi.org/10.1524/ncrs.1997.212.1.457.
(22) Fan, H.-L.; Cao, M.-H.; QI, Y.-J.; Mao, L.; Hu, C.-W.; Wang, E.-B. Hydrothermal Synthesis and Crystal Structure of a 3D Rare-earth Coordination Polymer $[Ce_2(H_2btc)(btc)(H_2O)_2]_n$. *Chem. J. Chin. Univ.* **2004**, *25* (8), 1419–1421.
(23) Usman, M.; Chibuike, M.; Patil, D.; Rigin, S.; Zhang, S.; Wu, Y.; Lindline, J.; Timofeeva, T. V. Magnetic Behaviour of 3D Metal−organic Frameworks Constructed via 1,2,4,5-Benzenetetracarboxylate Linker and 4f Ce(III) or 3d Fe(III) Metal Nodes. *Inorg. Chem. Commun.* **2020**, *122*, 108261. https://doi.org/10.1016/j.inoche.2020.108261.
(24) Ren, M.-J.; Zhang, Z.; Zhao, P.; Zhang, J. Three-dimensional Metal-Organic Hybrid Material Bearing an Open-Framework Self-Assembled by Mononuclear Cerium Benzene Tetracarboxylate Complex. *Asian J. Chem.* **2008**, *20*, 3687–3701.
(25) Li, X.; Wang, Y.; Ma, Z.; Zhang, R.; Zhao, J. Synthesis and Characterization of Two 3-D Polymeric Lanthanide Complexes Constructed from 1,2,4,5-Benzenetetracarboxylic Acid. *J. Coord. Chem.* **2010**, *63* (6), 1029–1037. https://doi.org/10.1080/00958971003690439.
(26) Li, C. Y.; Cai, D. M.; Yin, J. C.; Cai, L. P.; Zeng, M.; Wang, J.; Zhu, W. H. Crystal Structure, Fluorescence Spectroscopy, and Electrochemical Property of Two Neodymium Coordination Polymers with Phenoxy Acids. *Russ. J. Coord. Chem.* **2016**, *42* (7), 476–485. https://doi.org/10.1134/S107032841606004X.
(27) Dai, Y.-M.; Wang, X.-Q.; Huang, J.-F. Poly[Diaqua(μ_6-Benzene-1,2,4,5-Tetracarboxylato)(μ_6-2,5-Dicarboxybenzene-1,4-Dicarboxylato)Disamarium]. *Acta Crystallogr. E Struct. Rep. Online* **2005**, *61* (12), m2548–m2549. https://doi.org/10.1107/S1600536805036081.
(28) Tabatabaee, M.; Mohammadinasab, R.; Aghaie, M. A Three-Dimensional Samarium Coordination Polymer with Benzene-1,2,4,5-Tetracarboxylic Acid, Synthesis, Characterization and Thermal Decomposition to Sm_2O_3 Nanoparticles. *J. Inorg. Organomet. Polym.* **2016**, *26* (1), 127–133. https://doi.org/10.1007/s10904-015-0292-4.
(29) Wu, C.-D.; Lu, C.-Z.; Yang, W.-B.; Lu, S.-F.; Zhuang, H.-H.; Huang, J.-S. The Structure and Physical Properties of a Novel Three-Dimensional Zeolite-Like Nanoporous

Architecture Formed by Two Different Polymeric Layers: [Eu_2(Btc)(H_2btc)(H_2O)]·4H_2O. *Eur. J. Inorg. Chem.* **2002**, *2002* (4), 797–800. https://doi.org/10.1002/1099-0682(200203)2002:4<797::AID-EJIC797>3.0.CO;2-V.

(30) Cañadillas-Delgado, L.; Pasán, J.; Fabelo, O.; Julve, M.; Lloret, F.; Ruiz-Pérez, C. A Step Further in the Comprehension of the Magnetic Coupling in Gadolinium(III)-Based Carboxylate Complexes. *Polyhedron* **2013**, *52*, 321–332. https://doi.org/10.1016/j.poly.2012.09.016.

(31) Cao, R.; Sun, D.; Liang, Y.; Hong, M.; Tatsumi, K.; Shi, Q. Syntheses and Characterizations of Three-Dimensional Channel-like Polymeric Lanthanide Complexes Constructed by 1,2,4,5-Benzenetetracarboxylic Acid. *Inorg. Chem.* **2002**, *41* (8), 2087–2094. https://doi.org/10.1021/ic0110124.

(32) Luo, Z.-R.; Liao, L.-S.; Yin, X.-H. Hydrothermal Synthesis and Structural Studies of Two New Coordination Polymer of Gadolinium (III) and Erbium(III) with Benzene-1,2,4,5-Tetracarboxylic Acid. *Synth. React. Inorg. Met. Org. Nano Met. Chem.* **2014**, *44* (8), 1086–1091. https://doi.org/10.1080/15533174.2013.797462.

(33) Bai, W.-W.; Zhu, N.; Han, L.-M.; Hong, H.-L.; Gao, Y.-Y.; Suo, Q.-L. *Chin. J. Struct. Chem.* **2012**, *31*, 1021.

(34) Hu, M.; Zhu, N.; Li, X.; Chen, F. Hydrothermal Synthesis and Structure of a Novel Terbium Coordination Polymer with Packing Cavities, {[Tb$(TCB)_{1/2}$($H_2TCB)_{1/2}$(H_2O)]($H_2O)_2$}$_n$ (H_2TCB = 1, 2, 4, 5-benzenetetracarboxylic Acid). *Cryst. Res. Technol.* **2004**, *39* (6), 505–510. https://doi.org/10.1002/crat.200310218.

(35) Lee, L.-W.; Pao, S.-Y.; Pathak, A.; Kang, D.-Y.; Lu, K.-L. Membrane Adsorber Containing a New Sm(III)–Organic Framework for Dye Removal. *Environ. Sci.: Nano* **2019**, *6* (4), 1067–1076. https://doi.org/10.1039/C9EN00018F.

(36) Lahoud, M. G.; Frem, R. C. G.; Marques, L. F.; Arroyos, G.; Brandão, P.; Ferreira, R. A. S.; Carlos, L. D. A Novel near Monochromatic Red Emissive Europium(III) Metal-Organic Framework Based on 1,2,4,5-Benzenetetracarboxylate: From Synthesis to Photoluminescence Studies. *J. Solid State Chem.* **2017**, *253*, 176–183. https://doi.org/10.1016/j.jssc.2017.05.041.

(37) Yang, J.-J.; Yu, X.-Y.; Luo, Y.-H.; Zhang, H.; Gao, W.-P. Three Unprecedented High-Connected 3D Lanthanide–Organic Frameworks Based on Benzene-1,2,4,5-Tetracarboxylic Acid. *Inorg. Chem. Comm.* **2015**, *61*, 16–20. https://doi.org/10.1016/j.inoche.2015.08.012.

(38) Qiao, W.-T.; Zhao, D.; Ma, F.-X. Crystal Structure of Poly[Octaaqua-Tris(Benzene-1,2,4,5-Tetracarboxylato)Tetralanthanum(III)] Hexahydrate, $C_{30}H_{34}La_4O_{38}$. *Z. Kristallogr. NCS* **2016**, *231* (1), 289–291. https://doi.org/10.1515/ncrs-2015-0125.

(39) Zhao, X.-Y.; Wang, J.; Yang, Q.-S.; Fu, D.-L.; Jiang, D.-K. A Hydrostable Samarium(III)-MOF Sensor for the Sensitive and Selective Detection of Tryptophan Based on a "Dual Antenna Effect." *Anal. Methods* **2021**, *13* (35), 3994–4000. https://doi.org/10.1039/D1AY01050F.

(40) Zhao, X.-Y. *CSD Communication CCDC 2087956* **2021**.

(41) Daiguebonne, C.; Deluzet, A.; Camara, M.; Boubekeur, K.; Audebrand, N.; Gérault, Y.; Baux, C.; Guillou, O. Lanthanide-Based Molecular Materials: Gel Medium Induced Polymorphism. *Cryst. Growth Des.* **2003**, *3* (6), 1015–1020. https://doi.org/10.1021/cg020060b.

(42) Luo, Y.; Bernot, K.; Calvez, G.; Freslon, S.; Daiguebonne, C.; Guillou, O.; Kerbellec, N.; Roisnel, T. 1,2,4,5-Benzene-Tetra-Carboxylic Acid: A Versatile Ligand for High Dimensional Lanthanide-Based Coordination Polymers. *CrystEngComm* **2013**, *15* (10), 1882. https://doi.org/10.1039/c2ce26940f.

(43) Wang, Y.-B.; Zhuang, W.-J.; Jin, L.-P.; Lu, S.-Z. New Lanthanide Coordination Polymers of 1,2,4,5-Benzenetetracarboxylic Acid and 4,4′-Bipyridine with 1D Channels. *J. Mol. Struct.* **2005**, *737* (2–3), 165–172. https://doi.org/10.1016/j.molstruc.2004.10.062.
(44) Amombo Noa, F. M.; Abrahamsson, M.; Ahlberg, E.; Cheung, O.; Göb, C. R.; McKenzie, C. J.; Öhrström, L. A Unified Topology Approach to Dot-, Rod-, and Sheet-MOFs. *Chem* **2021**, *7* (9), 2491–2512. https://doi.org/10.1016/j.chempr.2021.07.006.
(45) Liang, X.; Fan, Z.-I. Structural Characterization and Proton-conductive Property of a Lanthanide Metal-Organic Framework Assembled from 1,2,4,5-Benzenetetracarboxylic Acid and Piperazine. *Chin. J. Struct. Chem.* **2017**, *36*, 977.
(46) Zhang, R.-H.; Zhao, D.; Li, F.-F.; Fan, Y.-C.; Liu, B.-G. Catena-(Formyl(dimethyl)ammonium(μ^6-Benzene-1,2,4,5-Tetracarboxylato)-(μ^5-hydrogenBenzen-1,2,4,5-Tetracarboxylato)-triaqua-di-lanthanum). *Chin. J. Struct. Chem.* **2015**, *34*, 938.
(47) Feyisa Bogale, R.; Ye, J.; Sun, Y.; Sun, T.; Zhang, S.; Rauf, A.; Hang, C.; Tian, P.; Ning, G. Highly Selective and Sensitive Detection of Metal Ions and Nitroaromatic Compounds by an Anionic Europium(III) Coordination Polymer. *Dalton Trans.* **2016**, *45* (27), 11137–11144. https://doi.org/10.1039/C6DT01636G.
(48) Feyisa Bogale, R.; Chen, Y.; Ye, J.; Zhang, S.; Li, Y.; Liu, X.; Zheng, T.; Rauf, A.; Ning, G. A Terbium(III)-Based Coordination Polymer for Selective and Sensitive Sensing of Nitroaromatics and Ferric Ion: Synthesis, Crystal Structure and Photoluminescence Properties. *New J. Chem.* **2017**, *41* (21), 12713–12720. https://doi.org/10.1039/C7NJ02492D.
(49) Xue, D.-X.; Cairns, A. J.; Belmabkhout, Y.; Wojtas, L.; Liu, Y.; Alkordi, M. H.; Eddaoudi, M. Tunable Rare-Earth Fcu-MOFs: A Platform for Systematic Enhancement of CO_2 Adsorption Energetics and Uptake. *J. Am. Chem. Soc.* **2013**, *135* (20), 7660–7667. https://doi.org/10.1021/ja401429x.
(50) Xue, D.-X.; Belmabkhout, Y.; Shekhah, O.; Jiang, H.; Adil, K.; Cairns, A. J.; Eddaoudi, M. Tunable Rare Earth **Fcu** -MOF Platform: Access to Adsorption Kinetics Driven Gas/Vapor Separations via Pore Size Contraction. *J. Am. Chem. Soc.* **2015**, *137* (15), 5034–5040. https://doi.org/10.1021/ja5131403.
(51) Vizuet, J. P.; Mortensen, M. L.; Lewis, A. L.; Wunch, M. A.; Firouzi, H. R.; McCandless, G. T.; Balkus, K. J. Fluoro-Bridged Clusters in Rare-Earth Metal–Organic Frameworks. *J. Am. Chem. Soc.* **2021**, *143* (43), 17995–18000. https://doi.org/10.1021/jacs.1c10493.
(52) Zhao, Y.; Wang, C.-A.; Li, J.-K.; Li, Q.-L.; Guo, Q.; Ru, J.; Ma, C.-L.; Han, Y.-F. A Eu(III) Metal–Organic Framework Based on Anthracenyl and Alkynyl Conjugation as a Fluorescence Probe for the Selective Monitoring of Fe^{3+} and TNP. *RSC Adv.* **2022**, *12* (41), 26945–26952. https://doi.org/10.1039/D2RA02892A.
(53) SAINT Plus Version 8.34a, Bruker Analytical X-Ray Systems. *Brucker Analytical X-ray Systems: Madison, WI, 2008*. MADISON, WI. 2014.
(54) Sheldrick, G. M. SADABS, Bruker-Siemens Area Detector Absorption and Other Correction, Version 2014/5. *Brucker-Siemens Area detector Absorption and Other Correction*. Bruker, MADISON, WI 2015.
(55) Dolomanov, O. V.; Bourhis, L. J.; Gildea, R. J.; Howard, J. A. K.; Puschmann, H. *OLEX2* : A Complete Structure Solution, Refinement and Analysis Program. *J. Appl. Crystallogr.* **2009**, *42* (2), 339–341. https://doi.org/10.1107/S0021889808042726.
(56) Materials Studio, BIOVIA, San Diego. *Materials Studio, BIOVIA, San Diego*. 2020.
(57) Abascal, J. L. F.; Vega, C. A General Purpose Model for the Condensed Phases of Water: TIP4P/2005. *J. Chem. Phys.* **2005**, *123* (23), 234505. https://doi.org/10.1063/1.2121687.

(58) Düren, T.; Millange, F.; Férey, G.; Walton, K. S.; Snurr, R. Q. Calculating Geometric Surface Areas as a Characterization Tool for Metal−Organic Frameworks. *J. Phys. Chem. C* **2007**, *111* (42), 15350–15356. https://doi.org/10.1021/jp074723h.
(59) Rosi, N. L.; Kim, J.; Eddaoudi, M.; Chen, B.; O'Keeffe, M.; Yaghi, O. M. Rod Packings and Metal−Organic Frameworks Constructed from Rod-Shaped Secondary Building Units. *J. Am. Chem. Soc.* **2005**, *127* (5), 1504–1518. https://doi.org/10.1021/ja045123o.
(60) Liu, X.; Wang, X.; Gao, T.; Xu, Y.; Shen, X.; Zhu, D. Three 3D Lanthanide–Organic Frameworks with Sra Topology: Syntheses, Structures, Luminescence and Magnetic Properties. *CrystEngComm* **2014**, *16* (13), 2779. https://doi.org/10.1039/c3ce42553c.
(61) Blatov, V. A.; Carlucci, L.; Ciani, G.; Proserpio, D. M. Interpenetrating Metal–Organic and Inorganic 3D Networks: A Computer-Aided Systematic Investigation. Part I. Analysis of the Cambridge Structural Database. *CrystEngComm* **2004**, *6* (65), 377–395. https://doi.org/10.1039/B409722J.
(62) Loiseau, T.; Serre, C.; Huguenard, C.; Fink, G.; Taulelle, F.; Henry, M.; Bataille, T.; Férey, G. A Rationale for the Large Breathing of the Porous Aluminum Terephthalate (MIL-53) Upon Hydration. *Chem. Eur. J.* **2004**, *10* (6), 1373–1382. https://doi.org/10.1002/chem.200305413.
(63) Burrows, A. D.; Cassar, K.; Friend, R. M. W.; Mahon, M. F.; Rigby, S. P.; Warren, J. E. Solvent Hydrolysis and Templating Effects in the Synthesis of Metal–Organic Frameworks. *CrystEngComm* **2005**, *7* (89), 548. https://doi.org/10.1039/b509460g.
(64) Chatenever, A. R. K.; Warne, L. R.; Matsuoka, J. E.; Wang, S. J.; Reinheimer, E. W.; LeMagueres, P.; Fei, H.; Song, X.; Oliver, S. R. J. Isomorphous Lanthanide Metal–Organic Frameworks Based on Biphenyldicarboxylate: Synthesis, Structure, and Photoluminescent Properties. *Cryst. Growth Des.* **2019**, *19* (8), 4854–4859. https://doi.org/10.1021/acs.cgd.9b00840.
(65) Wang, M.; Zeng, G.; Zhang, X.; Bai, F. Y.; Xing, Y. H.; Shi, Z. A New Family of Ln-BTC-AC-FM Framework Intelligent Materials: Precise Synthesis, Structure and Characterization for Fluorescence Detecting of UO22+ and Adsorbing Dyes. *J. Mol. Struct.* **2021**, *1238*, 130422. https://doi.org/10.1016/j.molstruc.2021.130422.
(66) Mihalcea, I.; Henry, N.; Loiseau, T. Crystal Chemistry of Uranyl Carboxylate Coordination Networks Obtained in the Presence of Organic Amine Molecules. *Eur. J. Inorg. Chem.* **2014**, *2014* (8), 1322–1332. https://doi.org/10.1002/ejic.201301575.
(67) Kole, G. K.; Vittal, J. J. Solid-State Reactivity and Structural Transformations Involving Coordination Polymers. *Chem. Soc. Rev.* **2013**, *42* (4), 1755–1775. https://doi.org/10.1039/C2CS35234F.
(68) He, W.-W.; Li, S.-L.; Lan, Y.-Q. Liquid-Free Single-Crystal to Single-Crystal Transformations in Coordination Polymers. *Inorg. Chem. Front.* **2018**, *5* (2), 279–300. https://doi.org/10.1039/C7QI00724H.
(69) Férey, G.; Serre, C. Large Breathing Effects in Three-Dimensional Porous Hybrid Matter: Facts, Analyses, Rules and Consequences. *Chem. Soc. Rev.* **2009**, *38* (5), 1380. https://doi.org/10.1039/b804302g.
(70) Schneemann, A.; Bon, V.; Schwedler, I.; Senkovska, I.; Kaskel, S.; Fischer, R. A. Flexible Metal–Organic Frameworks. *Chem. Soc. Rev.* **2014**, *43* (16), 6062–6096. https://doi.org/10.1039/C4CS00101J.
(71) Serre, C.; Mellot-Draznieks, C.; Surblé, S.; Audebrand, N.; Filinchuk, Y.; Férey, G. Role of Solvent-Host Interactions That Lead to Very Large Swelling of Hybrid Frameworks. *Science* **2007**, *315* (5820), 1828–1831. https://doi.org/10.1126/science.1137975.
(72) Shirsat, A. N.; Ali, M.; Kaimal, K. N. G.; Bharadwaj, S. R.; Das, D. Thermochemistry of $La_2O_2CO_3$ Decomposition. *Thermochim. Acta* **2003**, *399* (1–2), 167–170. https://doi.org/10.1016/S0040-6031(02)00459-8.

For Table of Content Only

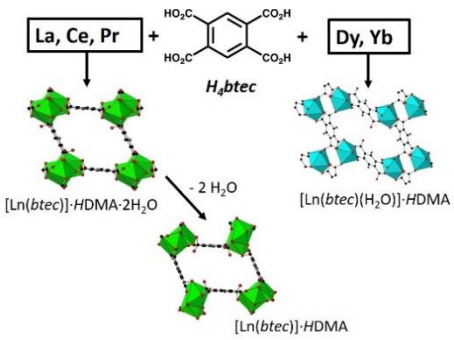

Lanthanides (La, Ce, Pr, Dy, Yb) coordination by pyromellitate ligands leads to the formation of 3D coordination polymers showing a crystal-to-crystal transformation upon dehydration with a pore volume decrease of about 6%.